5-1-2011

Abundances of Stars with Planets: Trends with Condensation Temperature

Simon C. Schuler
National Optical Astronomy Observatory

Davin Flateau
University of Cincinnati

Katia Cunha
National Optical Astronomy Observatory

Jeremy R. King
Clemson University, jking2@clemson.edu

Luan Ghezzi
Observatorio Nacional, Rua General Jose Cristano

See next page for additional authors

Authors
Simon C. Schuler, Davin Flateau, Katia Cunha, Jeremy R. King, Luan Ghezzi, and Verne V. Smith

The Astrophysical Journal, 732:55 (15pp), 2011 May 1 doi:10.1088/0004-637X/732/1/55

ABUNDANCES OF STARS WITH PLANETS: TRENDS WITH CONDENSATION TEMPERATURE*,†

Simon C. Schuler[1,7], Davin Flateau[2], Katia Cunha[1,3,4], Jeremy R. King[5], Luan Ghezzi[3,6], and Verne V. Smith[1]
[1] National Optical Astronomy Observatory, 950 North Cherry Avenue, Tucson, AZ 85719, USA; sschuler@noao.edu, kcunha@noao.edu, vsmith@noao.edu
[2] Department of Physics, University of Cincinnati, Cincinnati, OH 45221, USA; flateadc@mail.uc.edu
[3] Observatório Nacional, Rua General José Cristino, 77, 20921-400 São Cristóvão, Rio de Janeiro, RJ, Brazil; luan@on.br
[4] Steward Observatory, University of Arizona, 933 North Cherry Avenue, Tucson, AZ 85721, USA
[5] Department of Physics and Astronomy, Clemson University, 118 Kinard Laboratory, Clemson, SC 29634, USA; jking2@clemson.edu
[6] Laboratório Interinstitucional de e-Astronomia, - LlneA, Rua Gal. José Cristino 77, Rio de Janeiro, RJ-20921-400, Brazil
Received 2010 December 17; accepted 2011 March 2; published 2011 April 14

ABSTRACT

Precise abundances of 18 elements have been derived for 10 stars known to host giant planets from high signal-to-noise ratio, high-resolution echelle spectroscopy. Internal uncertainties in the derived abundances are typically $\lesssim$0.05 dex. The stars in our sample have all been previously shown to have abundances that correlate with the condensation temperature (T_c) of the elements in the sense of increasing abundances with increasing T_c; these trends have been interpreted as evidence that the stars may have accreted H-depleted planetary material. Our newly derived abundances also correlate positively with T_c, although slopes of linear least-square fits to the [m/H]–T_c relations for all but two stars are smaller here than in previous studies. When considering the refractory elements ($T_c > 900$ K) only, which may be more sensitive to planet formation processes, the sample can be separated into a group with positive slopes (four stars) and a group with flat or negative slopes (six stars). The four stars with positive slopes have very close-in giant planets (three at 0.05 AU) and slopes that fall above the general Galactic chemical evolution trend. We suggest that these stars have accreted refractory-rich planet material but not to the extent that would increase significantly the overall stellar metallicity. The flat or negative slopes of the remaining six stars are consistent with recent suggestions of a planet formation signature, although we show that the trends may be the result of Galactic chemical evolution.

Key words: planetary systems – planets and satellites: formation – stars: abundances – stars: atmospheres

Online-only material: machine-readable tables

1. INTRODUCTION

The primary objective of chemical abundance studies of planetary host stars is to identify possible vestiges of the planet formation process that will lead to a greater understanding of how planets form and evolve. The validity of this endeavor was verified shortly after the discovery of the first planet orbiting a solar-type star (Mayor & Queloz 1995) when Gonzalez (1997, 1998) found that host stars, in general, have larger Fe abundances than stars without known planets. The metal-rich nature of stars with giant planets has been confirmed by various groups (e.g., Santos et al. 2001; Fischer & Valenti 2005; Ghezzi et al. 2010b), and substantial observational evidence indicates that it is an intrinsic property of these planetary systems (e.g., Fischer & Valenti 2005; Ghezzi et al. 2010a). Core-accretion models of planet formation (e.g., Ida & Lin 2004) naturally account for this giant planet–metallicity correlation.

An alternative explanation for the enhanced metallicities of stars with giant planets was proposed by Gonzalez (1997). He suggested that the metallicities of the host stars are not primordial but are the result of self-enrichment, i.e., the accretion of H-depleted material onto the star as a result of dynamical processes in the protoplanetary disk. Gonzalez postulated that if stars with planets accrete fractionated disk material, their photospheric abundances should correlate with the condensation temperatures (T_c) of the elements such that high-T_c refractory elements are more abundant than low-T_c volatile elements. Whereas the infall of planetary debris onto host stars may be a common occurrence in planet-forming disks (for a review, see Li et al. 2008), it is unclear from modeling efforts if accreted material would leave an observable imprint on a stellar photosphere (Pinsonneault et al. 2001; Murray & Chaboyer 2002; Vauclair 2004). Attempts to identify trends with T_c (Smith et al. 2001; Ecuvillon et al. 2006a; Gonzalez 2006) resulted in finding no significant differences between stars with and without giant planets, although Smith et al. (2001, henceforth S01) and Ecuvillon et al. (2006a, henceforth E06) noted that small subsets of stars with planets stood out as having particularly strong correlations of increasing abundances with increasing T_c. Furthermore, S01 found that the stars with the strong correlations have planets that are on much closer orbits, on average, than stars not showing the possible abundance trend.

Meléndez et al. (2009, henceforth M09) revisited the idea that accretion of disk material, while maybe not the primary mechanism responsible for the observed enhanced metallicities, may imprint T_c trends in the photospheres of planet host stars, with results that are contrary to original expectations. They showed that the Sun is *deficient* in refractory elements relative to volatile elements when compared to the mean abundances of 11 solar twins (stars with stellar parameters that are nearly identical to those of the Sun) and that the abundance differences correlate strongly with T_c in the sense that the abundances decrease with increasing T_c. This trend is interpreted by the authors as a possible signature of terrestrial planet formation in the solar

* Based on observations with the High Resolution Spectrograph on the Hobby-Eberly Telescope, which is operated by McDonald Observatory on behalf of the University of Texas at Austin, Pennsylvania State University, Standford University, the Ludwig-Maximilians-Universität München, and the Georg-August-Universität, Göttingen.

† Based on observations made with the FEROS instrument on the MPG/ESO 2.2 m telescope at La Silla (Chile), under the agreement ESO-Observatório Nacional/MCT.

[7] Leo Goldberg Fellow.

system, suggesting that the refractory elements depleted in the solar photosphere are locked up in the terrestrial planets.

In a comparison of solar refractory abundances to the refractory abundances of solar twins and solar analogs (stars with stellar parameters similar to those of the Sun) it was found that ∼85% of the stars do not show the putative terrestrial planet signature, i.e., they are enhanced in refractory elements relative to the Sun (Ramírez et al. 2009, 2010). These studies speculate that the remaining ∼15% of the stars, which have abundance patterns similar to the Sun, are terrestrial planet hosts. Subsequently, Gonzalez et al. (2010) investigated the abundances of refractory elements versus T_c trends for a sample of stars with and without known giant planets. Stars with giant planets were found to have more negative trends (decreasing abundances with increasing T_c) than stars without known planets; moreover, the most metal-rich stars with giant planets have the most negative trends. These results potentially indicate that the depleted abundances of refractory elements in stellar photospheres are a consequence of both terrestrial and giant planet formation (Gonzalez et al. 2010). Recently, González Hernández et al. (2010) studied a sample of solar twins and analogs with and without planets and found similar abundance patterns for each sample, including two stars with terrestrial super-Earth-type planets; they have suggested that the abundance pattern identified by M09 may not be related to the planet formation. Ramírez et al. (2010) in turn pointed out that the analysis of González Hernández et al. (2010) included both volatile and refractory elements, and that the planet signature is more robust among the refractories. In a reanalysis of the González Hernández et al. data for the two stars with super-Earth-type planets, Ramírez et al. (2010) find abundance patterns consistent with the planet signature.

Here, we present precise abundances of 18 elements for 10 stars with known giant planets derived homogeneously from high-quality, high-resolution echelle spectroscopy. The target stars were taken from the aforementioned works of S01 and E06 and are a subset of those that were reported to have the strongest correlations of increasing abundances with increasing T_c. Thus, according to these studies, the stars are candidates for having accreted fractionated refractory-rich material. We compare our high-precision abundances to T_c, for all elements and for refractory elements ($T_c > 900$ K) only, to further investigate possible planet formation signatures.

2. OBSERVATIONS AND DATA REDUCTION

The stars studied here are distributed at both northern and southern declinations. Observations of the northern stars were carried out with the 9.2 m Hobby-Eberly Telescope (HET) and the High Resolution Spectrograph (HRS) at the McDonald Observatory. Eleven hours of queue observing time were allocated for this project by the National Optical Astronomy Observatory (NOAO) by way of the Telescope System Instrumentation Program (TSIP). Seven stars were observed on 13 separate nights, with four of the stars being observed on multiple nights. The HRS fiber-fed echelle spectrograph was configured with a standard configuration, using the central echelle and 316g5936 (316 grooves mm^{-1} and central wavelength $\lambda = 5936$ Å) cross-disperser settings. The 2″ fiber was used with no accompanying sky fiber, no image slicer, and no iodine gas cell. The detector is a 4096 × 4096 two E2V (2048 × 4096; 15 μm pixels) ccd mosaic providing nearly complete spectral coverage from 4660 to 5920 Å over 27 orders and 6060 to 7790 Å over 22 orders, with the inter-ccd spacing accounting for the 140 Å gap. Two pixel binning was used in the cross-dispersion direction, while no binning was used in the dispersion direction. To achieve the highest spectral resolution possible, the effective slit width was set to 0″.25 (projected to 2.1 pixels), providing a nominal resolution of $R = 120{,}000$. The actual achieved resolution, as measured by small emission features in the ThAr comparison spectra, is $R \approx 115{,}000$. Total exposure times ranged from 24 to 165 minutes, resulting in signal-to-noise (S/N) ratios of 600–800.

Table 1
Observing Log

Star	V	Telescope	Date (UT)	N	T_{exp} (s)
HD 2039	9.00	ESO	2007 Aug 28	2	1500
HD 20367	6.40	HET	2007 Mar 10	1	1560
			2007 Sep 28	1	1342
			2007 Oct 3	2	1560
HD 40979	6.73	HET	2007 Feb 27	2	1080
			2007 Feb 28	2	1080
HD 52265	6.30	HET	2007 Feb 27	2	1440
		ESO	2007 Apr 8	2	100
HD 75289	6.36	ESO	2007 Apr 7	2	100
HD 76700	8.13	ESO	2007 Apr 6	2	600
HD 89744	5.74	HET	2007 Mar 5	1	1740
HD 195019	6.91	HET	2007 May 10	2	1200
			2007 May 14	2	1200
HD 209458	7.65	HET	2007 Jun 8	2	1240
			2007 Jun 21	2	1240
			2007 Jul 16	2	1240
			2007 Aug 16	2	1240
HD 217107	6.18	HET	2007 Aug 10	2	1260

High-resolution echelle spectra of the southern targets were obtained with the 2.2 m MPG/ESO telescope and the Fiber-fed Extended Range Optical Spectrograph (FEROS) at the European Southern Observatory (ESO), La Silla under the agreement ESO-Observatório Nacional/MCT. These spectra have been used to determine stellar parameters, metallicities, and Li abundances of planetary host stars as presented by Ghezzi et al. (2010a, 2010b, 2010c), which should be consulted for a complete description of the observations and instrumental configuration. The ESO/FEROS spectra have an almost complete spectral coverage from 3560 to 9200 Å over 39 echelle orders and are characterized by a nominal resolution of $R \sim 48{,}000$ and S/N ratios of 330–400 at 6700 Å. All of the observations are summarized in an observing log presented in Table 1, and sample HET/HRS and ESO/FEROS spectra are given in Figure 1.

Data reduction was carried out separately for each data set. The HET/HRS spectra were reduced using standard techniques within the IRAF[8] image processing software. Calibration frames (biases, flat fields, ThAr comparison lamps, and telluric standards) were taken on every night, our objects were observed as part of the observatory's standard calibration plan. The reduction process included bias removal, scattered light subtraction, flat fielding, order extraction, and wavelength calibration. The FEROS Data Reduction System (DRS) was used to reduce the ESO/FEROS spectra, with the details provided by Ghezzi et al. (2010b).

3. ABUNDANCE ANALYSIS

The analysis of our high-quality data included spectroscopically determining stellar parameters (T_{eff}, $\log g$, and micro-

[8] IRAF is distributed by the National Optical Astronomy Observatory, which is operated by the Association of Universities for Research in Astronomy, Inc., under cooperative agreement with the National Science Foundation.

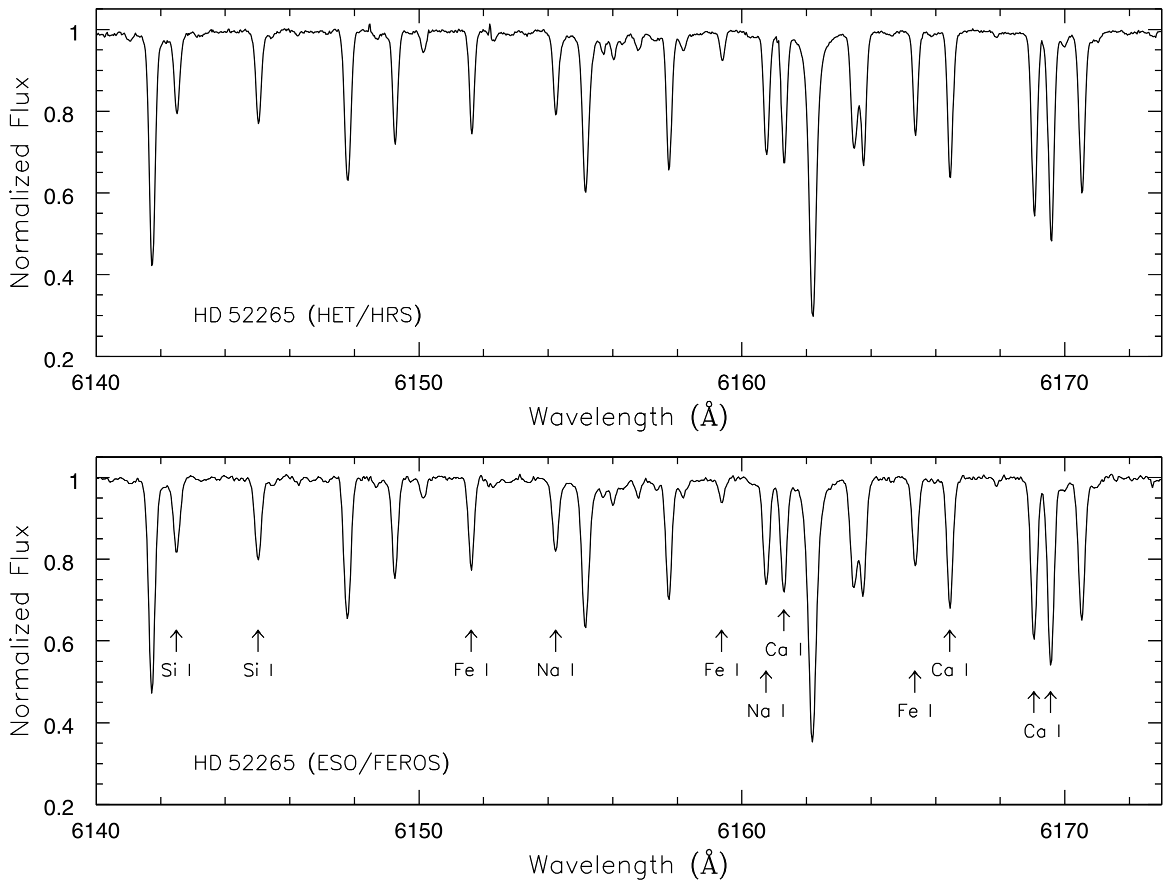

Figure 1. Sample spectra of HD 52265 obtained with HET/HRS (top) and ESO/FEROS (bottom). Lines for which EWs were measured are marked.

turbulence [ξ]) and deriving the abundances of 18 elements spanning condensation temperatures of 40–1659 K for each star. Abundances have been derived directly from equivalent width (EW) measurements of spectral lines and by the spectral synthesis method, depending on the spectral line being considered. The majority of EWs were measured by fitting Gaussian profiles to the lines, whereas some features, generally strong (EW $\geqslant$ 90 mÅ) lines with broader wings at the continuum, were fit with Voigt profiles. All EWs were measured using the one-dimensional spectrum analysis package SPECTRE (Fitzpatrick & Sneden 1987).

Abundances from the EW measurements and synthetic fits to the data were derived using an updated version of the LTE spectral analysis code MOOG (Sneden 1973). Model atmospheres have been interpolated from the Kurucz ATLAS9 grids[9] constructed assuming the convective overshoot approximation. The overshoot models are preferred, because of the finer grid steps available compared to the more up to date models with no overshoot and new opacity distribution functions. Furthermore, no significant differences ($\leqslant$0.05 dex) have been identified between abundances derived using the overshoot and no overshoot models for solar-metallicity open cluster dwarfs (e.g., Schuler et al. 2010), so the use of the overshoot models is not expected here to be an important source of error in the derived parameters and abundances.

3.1. Stellar Parameters

Stellar parameters for each star were derived using standard techniques. After adopting initial parameters from the literature (Santos et al. 2004), $T_{\rm eff}$, $\log g$, ξ, and [Fe/H] were altered and new [Fe/H] abundances derived until there existed zero correlation between [Fe I/H] and lower excitation potential (χ), and [Fe I/H] and reduced EW [log(EW/λ)], and also the [Fe/H] abundances derived from Fe I and Fe II lines were equal to within two significant digits. We note that unique solutions of $T_{\rm eff}$ and ξ are achieved only if there is no ab initio correlation between χ and EW of the Fe I lines analyzed; no significant correlation exists for our line list and measured EWs. The Fe lines measured were initially chosen from the extensive line list of Thevenin (1990). Each case "a" line was then visually inspected in a high-quality HET/HRS solar proxy spectrum (daytime sky spectrum; S/N $\sim$ 500 at $\sim$6700 Å) for potential blending, cosmic-ray contamination, proximity to order edges, or any other defect that may prevent the accurate measurement of a line. This process resulted in a final Fe line list containing 61 Fe I and 11 Fe II lines. We note that not all lines were measurable for each star in the sample. Atomic parameters (χ and transition probabilities [$\log gf$]) were obtained from the Vienna Atomic Line Database (VALD; Piskunov et al. 1995; Kupka et al. 1999; Ryabchikova et al. 1999) via email query. The [Fe/H] abundances of the target stars were normalized to solar values on a line-by-line basis. The line list with the adopted atomic parameters, and the EW measurements and resulting absolute abundances [log N(Fe)] for each star and the Sun are given in Table 2 for those observed with HET/HRS and Table 3 for those observed with ESO/FEROS.

Uncertainties in the stellar parameters are calculated by forcing 1σ correlations in the relations described above. For $T_{\rm eff}$, the uncertainty is the temperature change required to produce a correlation coefficient in [Fe I/H] versus χ significant at the

[9] See http://kurucz.harvard.edu/grids.html.

Table 2
Lines Measured, Equivalent Widths, and Abundances—HET/HRS

Ion	λ (Å)	χ (eV)	log *gf*	EW$_\odot$	log $N_\odot$	HD 20367 EW	HD 20367 log *N*	HD 40979 EW	HD 40979 log *N*	HD 52265 EW	HD 52265 log *N*
C I	5052.17	7.68	−1.304	33.1	8.46	42.1	8.44	55.0	8.57	55.8	8.60
	5380.34	7.68	−1.615	21.9	8.53	27.3	8.47	39.4	8.64	40.2	8.68
	6587.61	8.54	−1.021	13.9	8.43	21.3	8.45	30.2	8.58	29.8	8.60
	7111.47	8.64	−1.074	10.1	8.41	17.7	8.49	21.7	8.52	22.1	8.56
	7113.18	8.65	−0.762	22.5	8.56	27.5	8.44	39.1	8.59	40.1	8.64
O I	6300.30	0.00	−9.717	5.5[a]	8.69[a]	4.3	8.71	6.0	8.85	...	...
	7771.94	9.15	0.369	66.8	8.80	101.7	8.94	119.2	9.08	108.8	9.00
	7774.17	9.15	0.223	58.8	8.81	88.8	8.93	106.3	9.07	97.4	9.00
	7775.39	9.15	0.001	45.5	8.80	70.0	8.89	85.3	9.02	79.2	8.97
Na I	5682.63	2.10	−0.700	96.2	6.13	90.8	6.24	...	...	...	...
	6154.23	2.10	−1.560	36.3	6.25	30.1	6.31	38.8	6.50	43.2	6.54
	6160.75	2.10	−1.260	56.0	6.23	47.2	6.28	62.0	6.52	62.6	6.50

Notes.
[a] Taken from Schuler et al. (2006).
† Line used for hfs tests.
(This table is available in its entirety in a machine-readable form in the online journal. A portion is shown here for guidance regarding its form and content.)

Table 3
Lines Measured, Equivalent Widths, and Abundances—ESO/FEROS

Ion	λ (Å)	χ (eV)	log *gf*	EW$_\odot$	log $N_\odot$	HD 2039 EW	HD 2039 log *N*	HD 52265 EW	HD 52265 log *N*	HD 75289 EW	HD 75289 log *N*	HD 76700 EW	HD 76700 log *N*
C I	5052.17	7.68	−1.304	32.8	8.45	53.8	8.70	57.9	8.62	55.4	8.57	50.0	8.76
	5380.34	7.68	−1.615	20.8	8.49	35.5	8.71	40.5	8.67	36.5	8.58	31.8	8.74
	6587.61	8.54	−1.021	15.3	8.48	30.0	8.74	...	...	27.8	8.53	22.8	8.69
	7113.18	8.65	−0.762	21.6	8.53	...	...	...	...	39.2	8.61	...	...
O I	6300.30	0.00	−9.717	5.3	8.66	7.8	8.88	...	...	5.8	8.70	10.4	8.90
	7771.94	9.15	0.369	71.3	8.87	96.5	9.05	109.7	8.96	108.1	8.98	77.8	9.01
	7774.17	9.15	0.223	60.9	8.85	88.0	9.08	97.2	8.95	94.4	8.95	68.7	9.01
	7775.39	9.15	0.001	44.6	8.78	70.4	9.05	81.5	8.96	73.5	8.87	56.8	9.02
Na I	5682.63	2.10	−0.700	105.9	6.22	...	...	117.2	6.53	...	...	...	...
	6154.23	2.10	−1.560	36.4	6.25	59.7	6.67	43.1	6.54	39.4	6.47	67.3	6.68
	6160.75	2.10	−1.260	57.9	6.26	80.7	6.63	64.0	6.51	58.4	6.44	86.4	6.62

Note. † Line used for hfs tests.
(This table is available in its entirety in a machine-readable form in the online journal. A portion is shown here for guidance regarding its form and content.)

1σ level, and similarly for ξ, the correlation between [Fe I/H] and the reduced EW. Determining the uncertainty in $\log g$ requires an iterative process, as thoroughly described in Bubar & King (2010). Briefly, because the difference in the Fe I and Fe II abundances is sensitive to changes in $\log g$, the uncertainty $\log g$ is related to the uncertainty in the Fe abundances. Accordingly, $\log g$ is altered until the difference in the [Fe I/H] and [Fe II/H] abundances equals the combined uncertainty in [Fe I/H] and [Fe II/H], which is the quadratic sum of the uncertainties in each individual abundance due to the adopted $T_{\rm eff}$ and ξ as well as in the uncertainty in the mean (σ_μ[10]) Fe I and Fe II abundances (the derivation of the abundance uncertainties is described below). The method is then iterated, this time propagating the initial difference in $\log g$ into the Fe abundance uncertainties. The final uncertainty in $\log g$ is then the difference between the adopted value and the one obtained from this second iteration.

The final parameters and their 1σ uncertainties are provided in Table 4. Also included in the table are the derived [Fe I/H] and [Fe II/H] abundances, along with the number of lines measured for each and the uncertainty in the mean abundances.

[10] $\sigma_\mu = \sigma/\sqrt{N-1}$, where σ is the standard deviation and N is the number of lines measured.

3.2. Abundances

Lines for elements other than Fe were identified initially from Thevenin (1990). Again, each line was inspected visually in our high-quality solar spectrum for blends and other defects, and only those that were deemed clean were included in the final line list. Additional sources were used for some elements to supplement the initial list: Asplund et al. (2005b) for C I; Mashonkina et al. (2007) for Ca I; Mashonkina et al. (2010) for Ti I and Ti II; Rich & Boesgaard (2009) for Ti II; Gilli et al. (2006) for Mn I and Co I, and Ecuvillon et al. (2004b) for Zn I. Unless noted below, atomic parameters for all of the lines analyzed are from VALD. The final line list, including each line's wavelength, χ, and $\log gf$, and the measured EW, and derived absolute abundance [$\log N$(m)] for each star are provided in Table 2 for those observed with HET/HRS and Table 3 for those observed with ESO/FEROS. Below we describe the procedures used for those elements that required additional attention beyond a direct EW analysis.

3.2.1. Carbon

Carbon abundances have been derived from atomic C I and molecular C_2 features. The C I lines all arise from high-

Table 4
Stellar Parameters

Star	$T_{\rm eff}$ (K)	σ (K)	log g	σ	ξ (km s^{-1})	σ (km s^{-1})	[Fe I/H]	N	σ_μ	[Fe II/H]	N	σ_μ
HD 20367	6128	33	4.52	0.09	1.78	0.11	0.124	61	0.005	0.119	11	0.011
HD 40979	6205	50	4.40	0.16	1.75	0.12	0.248	57	0.007	0.246	10	0.018
HD 52265H	6145	33	4.35	0.14	1.80	0.09	0.228	60	0.005	0.226	11	0.013
HD 89744	6196	43	3.89	0.15	1.81	0.11	0.230	49	0.007	0.231	9	0.013
HD 195019	5787	31	4.16	0.06	1.59	0.07	0.067	61	0.005	0.073	11	0.006
HD 209458	6075	33	4.37	0.11	1.86	0.14	0.021	57	0.005	0.023	11	0.009
HD 217107	5666	40	4.26	0.14	1.35	0.07	0.374	50	0.007	0.372	10	0.018
HD 2039	5947	39	4.38	0.17	1.60	0.08	0.294	55	0.006	0.293	11	0.018
HD 52265F	6173	41	4.40	0.16	2.04	0.13	0.209	44	0.005	0.206	8	0.021
HD 75289	6120	45	4.21	0.13	1.83	0.10	0.251	57	0.006	0.250	11	0.017
HD 76700	5726	28	4.22	0.15	1.40	0.06	0.384	49	0.005	0.379	7	0.015

excitation (χ = 7.68–8.65 eV) transitions and thus are expected to be susceptible to NLTE effects (e.g., Asplund 2005). However, the two lines from the lowest energy levels considered here (λ5052 and λ5380) have been shown to deviate only slightly from LTE in the Sun and have estimated NLTE corrections $\leqslant$0.05 dex (Asplund et al. 2005b). Takeda & Honda (2005) have investigated NLTE corrections for these C I lines in 160 solar-type stars, with 5000 K $\leqslant T_{\rm eff} \leqslant$ 7000 K, and found the NLTE corrections on par with those found for the Sun, i.e., $\leqslant$0.05 dex. The stars in our sample are physically ($T_{\rm eff}$, log g, [Fe/H]) similar to those in the Takeda & Honda study, and thus comparably small NLTE corrections are expected for them. Consequently, any deviation from LTE should be negated in the solar-normalized [C/H] abundances derived from these lines.

Asplund (2005) suggests that C I lines arising from higher energy levels, including the remaining three (λ6588, λ7111, and λ7113) in our line list, should be more sensitive to NLTE effects; however, Asplund et al. (2005b) find corrections that are comparable to those for the λ5052 and λ5380 lines for the Sun. All of the C I lines analyzed here give comparable abundances for each star in our sample, with typical standard deviations of about 0.04 dex, except for HD 217107. For HD 217107, the two lower χ lines have a mean abundance [C/H] = 0.290 $\pm$ 0.028 (standard deviation), while the three higher χ lines have [C/H] = 0.463 $\pm$ 0.031 (s.d.). Measurement error is an unlikely source of the difference in these abundances given the quality of the data; NLTE effects are a more likely cause. HD 217107 is the most metal-rich star in our sample, and the Asplund et al. (2005b) results for the Sun may not be directly applicable to this star. We thus adopt the abundance from the two lower χ lines. We note that HD 76700 has a similarly high metallicity, as well as similar $T_{\rm eff}$ and log g, to HD 217107, and it does not demonstrate the discrepancy between the lower and higher χ lines. However, only one of the higher χ lines (λ6588) was measurable for this star. The C I lines analyzed, the EW measurements, and the absolute abundances are provided in Tables 2 and 3.

The C_2 lines at λ = 5086.3 and 5135.6 Å were also analyzed for abundances. These features are blends of multiple components of the C_2 system, so spectral synthesis was used for the abundance derivations. The line list is composed of atomic data from VALD and C_2 molecular data from Lambert & Ries (1981); the latter has been modified slightly from the original in order to fit the features in the Kurucz solar flux atlas (Kurucz et al. 1984) assuming a solar abundances of log $N_\odot$(C) = 8.39 (Asplund et al. 2005a). A C_2 dissociation energy of D_0 = 6.297 eV was assumed. The syntheses were smoothed to the appropriate resolution using a Gaussian broadening function; small unblended lines in the λ5086 and λ5135 regions were used to determine the full width half-maxima (FWHMs) of the Gaussian functions. Best fits of the synthesized spectra to the observed spectra were determined by eye.

Solar C abundances were derived by analyzing in the same way the C_2 features in our solar spectra, and the C_2-based solar-normalized abundances for each star are in excellent agreement with the abundances derived from the high-excitation C I lines, with differences $\leqslant$0.01 dex for the majority of the stars. The final adopted [C/H] abundances are the mean values of the individual C I- and C_2-based abundances for each line analyzed. A comparison of the derived C abundances is provided in Table 5.

3.2.2. Nitrogen

Nitrogen abundances were determined from spectral synthesis of the λ6703.9 and λ6704.0 blend, and the blend of λ6706.6 CN features in the λ6707 Li I region of our spectra. The Li line list from King et al. (1997) was revised and augmented with the CN data from Mandell et al. (2004). A CN dissociation energy of D_0 = 7.65 eV was assumed and the oscillator strengths of the features were adjusted to match the solar flux spectrum (Kurucz et al. 1984) with the input solar abundances of log N(C) = 8.39 and log N(N) = 7.78 (Asplund et al. 2005a). We note that our N abundances are differentially determined: the adopted solar abundance is used to calibrate the CN line list, and the resulting stellar N abundances are normalized with this same solar value. Concomitantly, these solar-normalized N abundances resulting from the weak features we utilize are independent of log gf value and the adopted solar C and N abundances.

Syntheses with varying N abundance were carried out using the mean C abundances described above and assuming an input Fe abundance corresponding to the mean value of [Fe/H]; this input Fe abundance was converted to an input absolute abundance assuming a solar value of log N(Fe) = 7.52 (adopted by MOOG; see Sneden et al. 1991). The resulting syntheses were smoothed using a rotational broadening function and v sin i values from the literature as well as a Gaussian broadening function to mimic instrumental broadening; the Gaussian FWHM was measured from unblended, well-defined emission features in ThAr calibration spectra. We also assumed macroturbulent broadening, which was set by forcing the synthetic line depths of the λ6703.5, λ6704.5, λ6705.1, and λ6710.3 Fe I features to match, overall, the observed depths after the rotational and instrumental broadening were fixed.

Table 5
Carbon and Oxygen Abundances

Star	[C I/H]	σ	[C$_2$/H]	σ	⟨[C/H]⟩[a]	N	σ_μ	[O I]	O I Triplet				
								[O/H]	[O/H]$_{\rm LTE}$	σ	[O/H]$_{\rm NLTE}$	σ	[O/H][a]
HD 20367	−0.02	0.08	+0.01	0.07	−0.01	7	0.03	+0.02	+0.11	0.02	+0.07	0.02	+0.02
HD 40979	+0.10	0.04	+0.10	0.06	+0.10	7	0.02	+0.16	+0.25	0.03	+0.18	0.02	+0.16
HD 52265H	+0.14	0.03	+0.14	0.01	+0.14	7	0.01	...	+0.18	0.01	+0.13	0.01	+0.13
HD 89744	+0.18	0.07	...	...	+0.18	5	0.03	...	+0.40	0.02	+0.22	0.01	+0.22
HD 195019	+0.08	0.04	+0.02	0.01	+0.06	7	0.02	+0.08	+0.11	0.01	+0.06	0.01	+0.08
HD 209458	−0.10	0.04	−0.10	0.05	−0.10	6	0.02	−0.04	+0.05	0.01	+0.01	0.02	−0.04
HD 217107	+0.29	0.03	+0.36	0.01	+0.32	7	0.02	+0.23	+0.24	0.01	+0.21	0.01	+0.23
HD 2039	+0.24	0.02	+0.25	0.01	+0.25	5	0.01	+0.22	+0.23	0.05	+0.19	0.03	+0.22
HD 52265F	+0.18	0.01	+0.19	...	+0.18	3	0.01	...	+0.13	0.03	+0.08	0.04	+0.08
HD 75289	+0.09	0.03	+0.08	0.01	+0.08	6	0.01	+0.04	+0.10	0.01	+0.01	0.01	+0.04
HD 76700	+0.26	0.05	+0.36	0.01	+0.30	5	0.03	+0.24	+0.28	0.07	+0.23	0.07	+0.24

Note. [a] Final adopted abundances.

Table 6
Abundances—HET/HRS

Element	HD 20367	HD 40979	HD 52265H	HD 89744	HD 195019	HD 209458	HD 217107
[C/H]	−0.01 ± 0.05	+0.10 ± 0.06	+0.14 ± 0.05	+0.18 ± 0.06	+0.06 ± 0.03	−0.10 ± 0.05	+0.32 ± 0.07
[N/H]	⩽+0.24	⩽+0.45	⩽+0.30	⩽+0.42	+0.05 ± 0.10	⩽+0.15	+0.49 ± 0.09
[O/H]	+0.02 ± 0.04	+0.16 ± 0.06	+0.13 ± 0.05	+0.22 ± 0.05	+0.08 ± 0.04	−0.04 ± 0.05	+0.23 ± 0.05
[Na/H]	+0.07 ± 0.03	+0.27 ± 0.04	+0.28 ± 0.02	+0.27 ± 0.03	+0.03 ± 0.03	+0.02 ± 0.04	+0.47 ± 0.04
[Mg/H]	+0.08 ± 0.02	+0.23 ± 0.05	+0.22 ± 0.05	+0.25 ± 0.03	+0.11 ± 0.03	+0.05 ± 0.03	+0.41 ± 0.04
[Al/H]	+0.03 ± 0.02	+0.21 ± 0.03	+0.21 ± 0.02	+0.25 ± 0.06	+0.07 ± 0.02	+0.04 ± 0.02	+0.44 ± 0.03
[Si/H]	+0.10 ± 0.01	+0.27 ± 0.02	+0.24 ± 0.02	+0.27 ± 0.02	+0.07 ± 0.01	+0.05 ± 0.02	+0.39 ± 0.02
[S/H]	+0.06 ± 0.05	+0.16 ± 0.05	+0.18 ± 0.05	+0.17 ± 0.04	+0.02 ± 0.03	...	+0.40 ± 0.09
[Ca/H]	+0.14 ± 0.03	+0.28 ± 0.05	+0.24 ± 0.04	+0.29 ± 0.05	+0.09 ± 0.03	+0.06 ± 0.04	+0.37 ± 0.05
[Sc/H]	+0.05 ± 0.04	+0.17 ± 0.08	+0.23 ± 0.07	+0.19 ± 0.07	+0.10 ± 0.05	+0.01 ± 0.05	+0.33 ± 0.07
[Ti/H]	+0.12 ± 0.06	+0.26 ± 0.09	+0.23 ± 0.08	+0.27 ± 0.10	+0.07 ± 0.05	+0.04 ± 0.07	+0.41 ± 0.08
[V/H]	+0.09 ± 0.04	+0.25 ± 0.05	+0.21 ± 0.03	+0.16 ± 0.05	+0.05 ± 0.03	0.00 ± 0.03	+0.37 ± 0.05
[Cr/H]	+0.12 ± 0.02	+0.26 ± 0.04	+0.22 ± 0.03	+0.21 ± 0.03	+0.06 ± 0.03	+0.04 ± 0.03	+0.39 ± 0.04
[Mn/H]	+0.04 ± 0.05	+0.23 ± 0.06	+0.21 ± 0.04	+0.16 ± 0.06	+0.00 ± 0.03	−0.07 ± 0.03	+0.38 ± 0.10
[Fe/H]	+0.12 ± 0.05	+0.25 ± 0.08	+0.23 ± 0.06	+0.23 ± 0.07	+0.07 ± 0.04	+0.02 ± 0.06	+0.37 ± 0.07
[Co/H]	+0.08 ± 0.03	+0.23 ± 0.04	+0.23 ± 0.03	+0.17 ± 0.05	+0.06 ± 0.03	−0.06 ± 0.03	+0.47 ± 0.04
[Ni/H]	+0.07 ± 0.03	+0.27 ± 0.04	+0.24 ± 0.02	+0.24 ± 0.04	+0.03 ± 0.02	−0.01 ± 0.03	+0.43 ± 0.03
[Zn/H]	+0.03 ± 0.06	+0.25 ± 0.07	+0.22 ± 0.05	+0.25 ± 0.07	+0.10 ± 0.03	−0.04 ± 0.05	+0.50 ± 0.03

N abundances were determined by minimizing the χ^2 values associated with the fit to the CN features. For the majority of our stars, only upper limits on the N abundance could be determined. The final N abundances and uncertainties are given in Tables 6 and 7.

3.2.3. Oxygen

Oxygen abundances have been derived from the forbidden [O I] line at $\lambda = 6300.3$ Å and the high-excitation O I triplet at $\lambda = 7771.9, 7774.2,$ and 7775.4 Å. Whereas the formation of the $\lambda 6300$ [O I] is well described by LTE (e.g., Takeda 2003), the O I triplet is highly sensitive to NLTE effects (e.g., Kiselman 1991; Asplund 2005). The extent of the effects has been shown to be dependent on metallicity, $T_{\rm eff}$, and $\log g$ (e.g., Nissen & Edvardsson 1992; Takeda 2003), with deviations from LTE becoming more severe for more metal-poor stars, increasing $T_{\rm eff}$, and decreasing $\log g$. The physical parameter space populated by some stars in our sample is such that NLTE effects are expected to be non-negligible, and for this reason, preference is given to [O I]-based abundances when possible.

Oxygen abundances were derived from the $\lambda 6300$ [O I] line using measured EWs and the `blends` driver in the MOOG package. By providing a line list that includes the blending lines and input abundances for the blending species, the `blends` driver accounts for the blending lines' contribution to the overall

Table 7
Abundances—ESO/FEROS

Element	HD 2039	HD 55265F	HD 75289	HD 76700
[C/H]	+0.25 ± 0.06	+0.18 ± 0.06	+0.08 ± 0.05	+0.30 ± 0.05
[N/H]	+0.41 ± 0.09	⩽+0.30	⩽+0.37	+0.48 ± 0.09
[O/H]	+0.22 ± 0.06	+0.08 ± 0.06	+0.04 ± 0.05	+0.24 ± 0.05
[Na/H]	+0.40 ± 0.05	+0.28 ± 0.04	+0.20 ± 0.04	+0.40 ± 0.06
[Mg/H]	+0.32 ± 0.06	+0.17 ± 0.06	+0.18 ± 0.04	...
[Al/H]	+0.32 ± 0.02	+0.22 ± 0.02	+0.29 ± 0.03	+0.48 ± 0.02
[Si/H]	+0.34 ± 0.02	+0.22 ± 0.02	+0.25 ± 0.02	+0.39 ± 0.01
[S/H]	+0.31 ± 0.06	+0.21 ± 0.05	+0.08 ± 0.04	+0.22 ± 0.04
[Ca/H]	+0.31 ± 0.04	+0.20 ± 0.04	+0.31 ± 0.04	+0.40 ± 0.04
[Sc/H]	+0.34 ± 0.07	+0.22 ± 0.07	+0.20 ± 0.05	+0.44 ± 0.06
[Ti/H]	+0.33 ± 0.09	+0.20 ± 0.09	+0.23 ± 0.08	+0.51 ± 0.08
[V/H]	+0.34 ± 0.04	+0.26 ± 0.04	+0.23 ± 0.05	+0.42 ± 0.04
[Cr/H]	+0.34 ± 0.03	+0.23 ± 0.03	+0.27 ± 0.03	+0.44 ± 0.03
[Mn/H]	+0.39 ± 0.04	+0.27 ± 0.05	+0.20 ± 0.07	+0.40 ± 0.08
[Fe/H]	+0.29 ± 0.08	+0.21 ± 0.08	+0.25 ± 0.07	+0.38 ± 0.07
[Co/H]	+0.32 ± 0.04	+0.27 ± 0.04	+0.21 ± 0.05	+0.51 ± 0.03
[Ni/H]	+0.35 ± 0.03	+0.23 ± 0.03	+0.26 ± 0.03	+0.45 ± 0.02
[Zn/H]	+0.32 ± 0.04	+0.16 ± 0.05	+0.09 ± 0.05	+0.46 ± 0.06

line strength of the feature when calculating the abundance of the primary element. In the case of the λ6300 [O I] line, the blending feature is a Ni I line consisting of two isotopic components (Johansson et al. 2003); here we adopt the weighted $\log gf$ values of the individual components as calculated by Bensby et al. (2004). For the [O I] line, we adopt the $\log gf$ value from the careful analysis of Allende Prieto et al. (2001). Spectral synthesis was also used for some stars to verify continuum placement and the `blends` results. The solar O abundance was derived from the [O I] line in the same way as the rest of the sample. However, the line in the HET/HRS solar spectrum is unusable due to obliteration by atmospheric emission. Therefore, the [O I] abundances of the stars observed with HET/HRS are normalized using a solar abundance of $\log N_{\odot}(\mathrm{O}) = 8.69$, the abundance derived in a previous study (Schuler et al. 2006) from a high-quality ($R = 60{,}000$ and S/N $\sim$ 950) daytime sky spectrum obtained with the Harlan J. Smith 2.7 m telescope. This spectrum is of higher quality than our ESO/FEROS solar spectrum and thus more comparable to our HET/HRS spectra. The measured EWs and absolute abundances of the [O I] line for the stars and the Sun are provided in Tables 2 and 3.

The O I triplet abundances were derived via an EW analysis assuming LTE. NLTE corrections from Takeda (2003), which provides an analytical formula to calculate the corrections for each line of the triplet, were applied to the LTE abundances of each star and the Sun. The Takeda (2003) formula has the functional form $\Delta = a10^{(b)(\mathrm{EW})}$, where a and b are coefficients that are functions of T_{eff} and $\log g$. Coefficients for these parameters that best match those of our sample stars were chosen. The resulting NLTE abundances are used primarily as a check of the [O I]-based abundances, but in the cases of HD 52265 and HD 89744, for which [O I] abundances are not available, the NLTE triplet abundances are adopted. The measured EWs and absolute abundances of the O I triplet lines are provided in Tables 2 and 3.

A comparison of the derived O abundances is shown in Table 5. The agreement between the [O I] and NLTE triplet abundances is quite good; the differences are $\leqslant$0.05 dex. This agreement provides confidence that the NLTE abundances adopted for HD 52265 and HD 89744 are reasonable.

3.2.4. Odd-Z Elements: Sc, V, Mn, and Co

For some odd-Z elements, electron–nucleus interactions can lead to significant hyperfine structure (hfs) in some transitions. The splitting of energy levels resulting from the hfs can produce increased line strengths that, if not properly treated, will lead to overestimated abundances (Prochaska & McWilliam 2000). Of the elements considered here, Sc, V, Mn, and Co are susceptible to the hfs, and as such, we have tested the EW-based abundances for these elements by using spectral synthesis incorporating hfs components to fit one Mn line and two lines each of Sc, V, and Co. The measured EWs and the non-hfs absolute abundances of these elements are provided in Tables 2 and 3, where the lines used for the hfs tests are marked.

The hfs components for the four elements are taken from Johnson et al. (2006), and the line lists for the regions surrounding each feature were obtained from VALD. The synthetic spectra were smoothed using a Gaussian broadening function, and the best fits to the observed spectra were again determined by eye. The same analysis was carried out for each solar spectrum, and the resulting solar abundances were used to normalize the hfs abundances of the stellar sample. Results from the hfs syntheses and comparisons to the EW-based abundances indicate that the differences between the two abundance determinations are negligible ($\leqslant$0.04 dex) for most stars. The two exceptions are the V and Mn abundances of HD 76700 and HD 217107, the two most metal-rich stars in the sample. Whereas the majority ($\sim$80%) of EWs for the four elements are $\leqslant$40 mÅ for each star, V and Mn lines have EWs > 60 mÅ and up to $\sim$100 mÅ for HD 76700 and HD 217107, line strengths that would be expected to have significant hfs (e.g., Prochaska & McWilliam 2000). The final adopted Sc, V, Mn, and Co abundances of all stars are those derived from the hfs analysis.

3.2.5. Abundance Uncertainties

Uncertainties in the derived abundances arise due to errors in the adopted stellar parameters as well as in the spread in abundances derived from individual lines of an element. The abundance uncertainties due to the stellar parameters are determined by first calculating the abundance sensitivities to the adopted parameters. Sensitivities were calculated for changes of $\pm$150 K in T_{eff}, $\pm$0.25 dex in $\log g$, and $\pm 0.30\ \mathrm{km\ s^{-1}}$ in ξ. In Table 8, we provide the abundance sensitivities for two stars, HD 20367 and HD 76700, as representative of the sample. We note that these two stars were observed with HET/HRS and ESO/FEROS, respectively. The abundance uncertainty due to each parameter is calculated by then scaling the sensitivities by the respective parameter uncertainty. The final total internal uncertainties (σ_{tot}) are the quadratic sum of the individual parameter uncertainties and the uncertainty in the mean, σ_{μ}, for those abundances derived from more than one line.

For N, three general contributions to the uncertainties in the derived abundances were considered: fitting uncertainties (which are well determined given the χ^2 approach and assumptions about the continuum level uncertainty), the direct effect of parameter errors on the N abundance itself (as described above), and the effect of uncertainties in the C abundances (which is a fixed input in the N analysis) on the derived N abundances. The final N abundance uncertainties are dominated by the direct effect of the T_{eff} uncertainty on the N abundance itself. The fitting uncertainties and the effect of uncertainties in $\log g$ on the input mean C abundance are also non-negligible contributors to the final total N uncertainties.

4. RESULTS AND DISCUSSION

The solar-normalized abundances and their uncertainties (σ_{tot}) for the stars observed with HET/HRS are provided in Table 6 and those observed with ESO/FEROS in Table 7. The uncertainties are all $\leqslant$0.10 dex and in most cases are $\leqslant$0.05 dex. A major factor in the low uncertainties is the collectively small standard deviations in the mean abundances—a testament to the quality of the spectra—for those elements derived from multiple lines. Also, the sensitivities of the abundances to changes in the stellar parameters are also relatively modest for most elements (Table 8).

Despite carrying out a homogeneous abundance analysis on the HET/HRS and ESO/FEROS data, differences in data quality and reduction techniques may lead to disparate abundance derivations. Results for HD 52265, the star observed by both telescopes, suggest that this is not the case here. The HET/HRS and ESO/FEROS abundances of this star are in excellent agreement, with a mean difference of 0.03 ± 0.02 (s.d.) dex. This further supports that our abundances are good to the $\sim$0.05 dex level.

Table 8
Abundance Sensitivities

Species	HD 20367			HD 76700		
	$\Delta T_{\rm eff}$ (±150 K)	$\Delta \log g$ (±0.25 dex)	$\Delta\xi$ (±0.30 km s^{-1})	$\Delta T_{\rm eff}$ (±150 K)	$\Delta \log g$ (±0.25 dex)	$\Delta\xi$ (±0.30 km s^{-1})
Fe I	±0.10	∓0.01	∓0.02	±0.09	∓0.01	∓0.05
Fe II	∓0.04	±0.11	∓0.03	∓0.07	±0.10	∓0.06
C I	∓0.09	±0.08	∓0.01	∓0.10	±0.06	∓0.01
N I	±0.22	∓0.01	±0.01	±0.24	±0.01	±0.01
O I	∓0.13	±0.07	∓0.03	∓0.16	±0.04	∓0.04
(O I)	$^{+0.01}_{-0.03}$	$^{+0.03}_{-0.05}$	$^{-0.01}_{-0.01}$	$^{+0.02}_{-0.01}$	$^{+0.11}_{-0.05}$	$^{+0.01}_{+0.01}$
Na I	±0.07	∓0.03	∓0.02	±0.08	∓0.03	∓0.03
Mg I	±0.07	∓0.03	∓0.03	±0.06	∓0.05	∓0.10
Al I	±0.07	∓0.01	∓0.01	±0.07	∓0.02	∓0.03
Si I	±0.04	∓0.01	∓0.02	±0.02	∓0.01	∓0.04
S I	∓0.05	±0.08	∓0.01	∓0.05	±0.07	∓0.01
Ca I	±0.10	∓0.03	∓0.06	±0.12	∓0.04	∓0.08
Sc II	±0.01	±0.10	∓0.02	∓0.01	±0.09	∓0.05
Ti I	±0.13	∓0.01	∓0.04	±0.15	∓0.01	∓0.10
Ti II	±0.01	±0.10	∓0.08	∓0.02	±0.07	∓0.13
V I	±0.14	∓0.02	∓0.01	±0.17	∓0.01	∓0.04
Cr I	±0.09	∓0.01	∓0.03	±0.11	∓0.02	∓0.07
Mn I	±0.13	∓0.01	∓0.02	±0.15	∓0.01	∓0.12
Co I	±0.12	±0.01	∓0.01	±0.12	±0.02	∓0.03
Ni I	±0.09	±0.01	∓0.03	±0.08	±0.01	∓0.07
Zn I	±0.05	±0.03	∓0.10	±0.01	±0.01	∓0.15

Abundances of the stars in our sample have been reported by numerous groups (e.g., Sadakane et al. 1999; Gonzalez & Laws 2000; Gonzalez et al. 2001; Takeda et al. 2001; Santos et al. 2004; Huang et al. 2005; Bond et al. 2006; Luck & Heiter 2006). In the following discussion, we focus on the two papers (and their sources) from which the stars in our sample were chosen, namely, S01 and E06.

S01 adopted the abundances of 29 stars from Gonzalez et al. (2001) and its preceding companion papers (Gonzalez 1998; Gonzalez & Laws 2000). Our sample includes four of these stars—HD 52265, HD 89744, HD 209458, and HD 217107. In general, the abundances from the two analyses are in good agreement, i.e., they agree within the combined uncertainties. One element that does merit discussion is C, a low-T_c element that, along with O, heavily influences the slope of the [m/H]–T_c relations. The C abundances of Gonzalez et al. (2001) are systematically lower than ours by about 0.10 dex, a difference that is not statistically significant but one that can dramatically affect the T_c slopes. The systematic difference cannot be ascribed to differences in the stellar parameters, nor should the difference be due to the adopted gf values since both analyses are done relative to solar abundances.[11] Each line list includes five C I lines, only two of which (λ5380 and λ6587) are used by both. For the two lines in common, the measured EWs are in reasonable agreement. We inspected the three remaining lines (λ7109, λ7115, and λ7117) used by Gonzalez et al. in our high-quality spectra, and both λ7109 and λ7115 appear to be blended with other lines. The blending is also apparent in the Kurucz solar flux atlas (Kurucz et al. 1984). We also consulted Thevenin (1990) and Asplund et al. (2005b), the sources of our C I line list, and none of the three remaining lines appear in those papers, further suggesting that the lines may not be suitable for precision abundance determinations. Although the systematic 0.10 dex offset between our C abundances and those of Gonzalez et al. (2001) cannot be explicitly attributed to the difference in the respective line lists, the use of the three blended red C I lines by Gonzalez et al. is a plausible source.

For the T_c analysis of E06, abundances were collected from multiple sources (Santos et al. 2004; Ecuvillon et al. 2004a, 2004b; Beirão et al. 2005; Ecuvillon et al. 2006b; Gilli et al. 2006). All 10 of the stars in our sample are included in these papers, although the same elements were not derived for all of the stars. The abundances used in E06 are in decent agreement with ours, with differences generally less than 0.15 dex and within the combined abundance uncertainties. However, some elements (Al, S, Ca, V, Zn, and Mn) do exhibit systematically divergent abundances on the order of ±0.10 dex for four or more stars. Again, differences in the derived stellar parameters cannot account for the systematic abundance differences, so the most probable source is other aspects of the abundance analyses, such as differences in the line lists, continuum placement, EW measurements, etc. The abundances of S and Zn are of particular interest, because they are both considered volatile elements ($T_c < 900$ K) and can affect the slope of the [m/H]–T_c relations. The S and Zn abundances reported in Ecuvillon et al. (2004b) are systematically lower than ours by about 0.15 and 0.08 dex, respectively. Similarly, in the comparison of their abundances to extant values in the literature, their S and Zn abundances are again lower for the majority of the stars (Ecuvillon et al. 2004b, Tables 14 and 15 therein).

4.1. Abundance Trends with T_c—Volatile and Refractory Elements

Similar to previous studies, we quantify the significance of an abundance trend with T_c by the slope of a standard linear least-squares fit. Fits weighted by the inverse variances of the solar-normalized abundances have also been made, but to be

[11] According to Gonzalez (1997) and Gonzalez & Laws (2000), the gf values of the spectral lines used by Gonzalez et al. (2001) are determined by an inverted analysis of the Sun adopting the solar abundances of Anders & Grevesse (1989, $\log N(\mathrm{C}) = 8.56$) and using the Kurucz solar flux atlas (Kurucz et al. 1984) and/or a solar-reflected spectrum of the asteroid Vesta; it is not clear from these sources which of the solar spectra was used for the C lines.

Table 9
Condensation Temperature of the Elements

Element	T_c [a] (K)
C	40
N	123
O	180
Na	958
Mg	1336
Al	1653
Si	1310
S	664
Ca	1517
Sc	1659
Ti	1582
V	1429
Cr	1296
Mn	1158
Fe	1334
Co	1352
Ni	1353
Zn	726

Note. [a] 50% condensation temperatures from Lodders (2003).

Table 10
Abundance Slopes with T_c

Star	Slope[a]	σ	Slope ($T_c > 900$ K)	σ
HD 20367	5.46	1.72	−0.51	5.27
HD 40979	6.52	2.09	−7.22	4.23
HD 52265H	5.41	1.36	−4.78	2.73
HD 89744	2.24	2.28	1.55	7.10
HD 195019	0.81	1.54	9.07	3.61
HD 209458	6.75	2.00	5.73	6.00
HD 217107	4.73	3.13	−9.06	5.70
HD 2039	4.88	1.85	−9.56	3.46
HD 52265F	5.19	2.22	−9.37	4.20
HD 75289	14.26	2.08	7.18	5.44
HD 76700	12.93	2.98	11.43	6.08

Note. [a] All values are $\times 10^{-5}$ dex K^{-1}.

consistent with the previous studies to which our results are compared (S01; E06; Gonzalez et al. 2010), the unweighted slopes are presented and discussed herein. We note however that the unweighted and weighted slopes for each star do not differ significantly, and the conclusions reached in this paper remain unchanged whether the unweighted or weighted slopes are considered, indicating that our results are robust. The fits are made to the abundances as a function of the 50% T_c from Lodders (2003; shown here in Table 9) calculated assuming a solar- system composition gas and a total pressure of 10^{-4} bar. The slopes of the fits are given in Table 10, and examples are shown in Figure 2. We note that the derived N abundances are not included in the calculation of the slopes because of the larger uncertainty in the N abundances and to maintain star-to-star consistency; definitive N measurements were possible for only four of the ten stars.

Positive slopes are found for all 10 stars, confirming the results of S01 and E06. However, for all but two stars (HD 75289 and HD 76700) our slope measurements are smaller than those of the previous studies, in most cases by more than a factor of two. The differences in the slopes are easily understood given the differences in the derived abundances described above. For example, the systematically lower C abundances derived by Gonzalez et al. (2001) and used by S01 are largely responsible for the more positive slopes of the latter. Differences in the abundances of other elements also contribute to the divergent slopes.

M09 and Ramírez et al. (2009, henceforth R09) have suggested that a precision of $\simeq$0.03 dex in abundance derivations is necessary to detect small differences in trends with T_c that might distinguish stars with and without planets. This, they argue, is why previous studies have not reached strong conclusions about the T_c-dependent abundances of planet host stars. This can also explain the differences in the calculated slopes seen here and those of S01 and E06. Whereas our abundance uncertainties are $\leqslant$0.05 dex, those reported in S01 and E06 are typically $\sim$0.10 dex or higher, resulting in larger uncertainties in the calculated slopes. The high quality of our data and the small abundance uncertainties should allow us to make firmer conclusions about the [m/H]–T_c slopes of our sample stars.

As initially suggested by Gonzalez (1997), a positive slope may indicate that the planetary host star has accreted fractionated rocky material as a consequence of planetary formation and evolution processes. Positive slopes also arise from general chemical evolution of Galactic disk stars, for instance by the observed trend of decreasing [O/Fe] ratios with increasing metallicities (e.g., Ramírez et al. 2007). The lower O abundances at higher metallicities will tend to make the [m/H]–T_c relations more positive. Indeed, S01 (Figure 10 therein) and E06 (Figure 3 therein) demonstrated the effects of chemical evolution on T_c slopes by comparing slopes of stars with and without known planets as a function of metallicity; both studies find a trend of increasing slopes with increasing metallicity, as expected. The 10 stars studied here were found by S01 and E06 to have slopes that fall above the scatter seen in their respective studies, and thus were inferred by the authors to have abundance patterns that deviate from those arising from general Galactic chemical evolution. At first sight, confirming the positive slopes for the 10 stars bolsters the conclusions of S01 and E06 that these stars may have accreted planetary material. However, the lower values of the slopes found here for seven stars (HD 20367, HD 40979, HD 52265, HD 89744, HD 195019, HD 217107, and HD 2039) place them in agreement with the Galactic chemical evolution trends found by S01 and E06. While firm conclusions cannot be drawn from a direct comparison of our slopes to the Galactic chemical evolution trends defined in S01 and E06 due to possible systematic differences arising from the different abundance analyses employed by each study, the smaller slopes found here seem to weaken the argument that these stars have accreted substantial amounts of planetary material. For the remaining stars, the slope for HD 209458 falls near the upper envelope of values for its metallicity, and those for HD 75289 and HD 76700 fall appreciably above the general Galactic trend. These three stars, especially the latter two, remain good candidates for having accreted fractionated rocky material.

4.2. Abundance Trends with T_c—Refractory Elements

R09 showed that the abundance trends of volatile elements in solar twins follow a similar pattern as the Sun and that these trends define the general chemical evolution of the Galaxy. The implication is that the Sun and other stars have retained the original volatile composition of the proto-stellar nebulae from which they formed. The abundance trends of the refractory

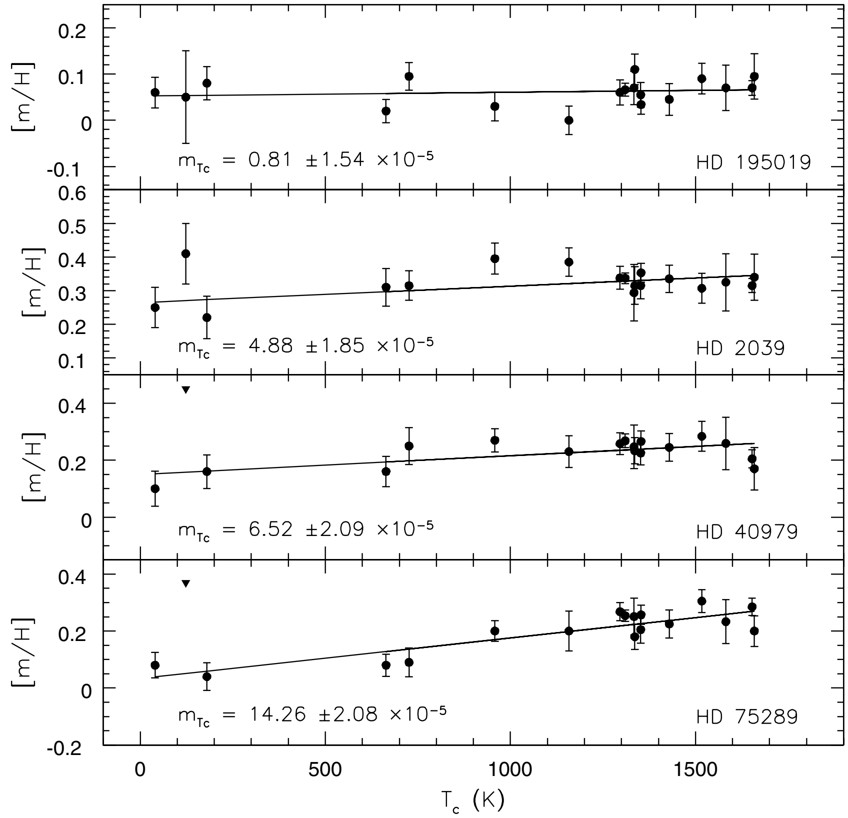

Figure 2. Relative abundances plotted against elemental condensation temperature, T_c, for four stars with planets. The solid line is a linear least-squares fit to the points. The slope and uncertainty of the fit are given in the lower left-hand corner of each window. Note that the N abundances (T_c = 123 K) are not included in the linear least-squares fit, as described in the text.

elements ($T_c > 900$ K), on the other hand, in $\simeq$85% of solar analogs were found to display a strong positive correlation with T_c. R09 attributed the increasing abundances with increasing T_c to the composition of refractory elements, which have been shown to be slightly depleted relative to volatile elements, in the Sun; this was interpreted as a possible signature of terrestrial planet formation in the solar system (M09). For the remaining $\simeq$15% of solar analogs, the T_c abundance trends of the refractory elements were found to be flat or have negative slopes, suggesting that their refractory element compositions are more similar to those of the Sun and are thus candidates for hosting terrestrial planets.

Following R09, we investigate the abundances of refractory elements ($T_c > 900$ K) as a function of T_c for our sample. The relations are again quantified by the slope of a standard linear least-squares fit to the data. The slopes of the fits are given in Table 10, and examples are shown in Figure 3. Whereas the [m/H]–T_c relations for all elements measured have positive slopes for each star, the slopes for the refractory elements seemingly can be placed into a group with positive slopes (four stars) and a group with flat or negative slopes (six stars). Of the four stars with positive slopes, one star (HD 209458) has a slope that is of the same order as its uncertainty and thus is also consistent with zero slope.

Positive slopes. In the interpretation of R09, stars that display positive [m/H]–T_c slopes are not terrestrial planet host candidates. M09 posited those stars with hot Jupiters that do not show the solar abundance pattern either accreted their fractionated gas disks while their convection zones were still deep and convective mixing erased the planet signature (i.e., enhanced volatiles) or interior planets had formed but had been subsequently accreted onto the star, enhancing the refractory abundances. Ramírez et al. (2010) conclude similarly, suggesting that the presence of hot Jupiters prevents the formation of terrestrial planets and consequently the appearance of the planet signature, or smaller planets may have already been accreted by the host stars. Future studies will be needed to determine how and if the formation of gas giants affects the formation of terrestrial planets; however, the accretion of refractory-rich planet cores may be a natural consequence of the constitution of hot Jupiter systems. Lin et al. (1996) showed that it is unlikely that gas giant planets can form near (0.05 AU) their host stars and that hot Jupiters formed at larger radii and subsequently migrated to their current locations as a result of angular momentum loss via tidal interactions with the surrounding disk (type I migration). Migrating gas giants can capture or clear planetary cores along their paths, potentially inducing the accretion of at least some of the cores onto the host star (Ida & Lin 2008).

The four stars with positive slopes—HD 75289, HD 76700, HD 195019, and HD 209458—are consistent with the accretion scenario. Properties of the planetary companions of the stars in our sample are provided in Table 11; the planetary data are from the Exoplanet Data Explorer.[12] As shown in Figure 4, the planets with the smallest semimajor axes are associated with the four positive slope stars (with exception of HD 217107 b, which is discussed below). Thus, the stars with the closest-in planets have positive [m/H]–T_c relations for the refractory elements. Also, HD 75289, HD 76700, and HD 209458, when the volatile and refractory elements are considered together, have slope values lying above the general Galactic evolution trend (as discussed

[12] Available at http://exoplanets.org.

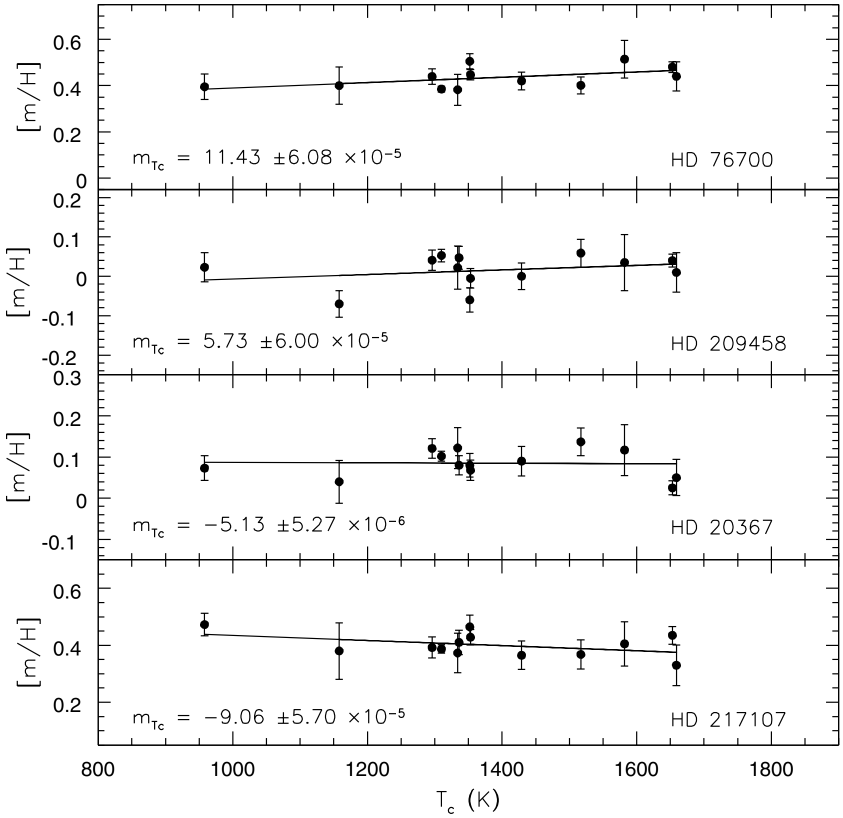

Figure 3. Relative abundances of refractory elements ($T_c > 900$ K) plotted against elemental condensation temperature for four stars with planets. The solid line is a linear least-squares fit to the points. The slope and uncertainty of the fit are given in the lower left-hand corner of each window.

Table 11
Planet Properties

Star	$M_{\sin i}$ (M_J)	Semimajor Axis (AU)	Period (days)	Eccentricity
HD 75289 b	0.5	0.05	3.5	0.03
HD 76700 b	0.2	0.05	4.0	0.10
HD 209458 b	0.7	0.05	3.5	0.00
HD 195019 b	3.6	0.14	18.2	0.01
HD 52265 b	1.1	0.50	119.3	0.33
HD 40979 b	4.0	0.85	264.1	0.25
HD 89744 b	8.5	0.92	256.8	0.67
HD 20367 b[a]	1.1	1.25	500.0	0.23
HD 2039 b	6.0	2.20	1120.0	0.72
HD 217107 c	2.6	5.33	4300.0	0.52
HD 217107 b	1.4	0.08	7.1	0.13

Note. [a] Data taken from the Extrasolar Planet Encyclopedia (available at http://exoplanet.eu). For all other stars, data taken from the Exoplanet Data Explorer (available at http://exoplanets.org).

in Section 4.1). It seems possible that these stars have accreted refractory-rich planet cores.

The magnitudes of the positive slopes found for the four stars are very similar to what would be obtained, for example, if $\sim$5 $M_\oplus$ of material having the bulk composition of the Earth (crust, mantle, and core; McDonough 2001) were mixed into the solar convective envelope ($m \sim 0.02\, M_\odot$) having a normal solar composition. Since convective envelope mass is a strong function of $T_{\rm eff}$, stars even slightly hotter than the Sun (say $\sim$6000 K) would require substantially less accreted material to create a measurable positive slope. However, the amount of accreted material necessary to produce the derived T_c slopes would not increase significantly the overall metallicity of the host star, supporting extant evidence that stars hosting giant planets are, on average, intrinsically more metal-rich than stars not known to host giant planets.

The case of HD 209458 is particularly interesting. This star is one of the brightest stars known to have a transiting planet, and it has been the focus of intense study. After the discovery of HD 209458 b (Henry et al. 2000; Charbonneau et al. 2000; Mazeh et al. 2000), subsequent radial velocity (Laughlin et al. 2005) and transit (Croll et al. 2007; Miller-Ricci et al. 2008) searches have not detected additional planets in this system. Also, a search for Trojan-type asteroids found no significance presence of such bodies in the system (Moldovan et al. 2010). It is not currently possible to know if additional planet cores were present when HD 209458 b formed and migrated to its current orbit, but the present lack of planets or other planetary material is intriguing in light of the accretion scenario.

Flat or negative slopes. The remaining six stars with flat or negative slopes, in the interpretation of R09, are possible hosts of terrestrial planets. M09 also considered if the formation of giant planets could be responsible for the planet signature. Four solar analogs with known close-in giant planets were included in their sample, but all of them were found to have abundance patterns that differ from the Sun. M09 concluded that the presence of close-in giant planets is not responsible for the planet signature, per se, and suggested that the difference could be due to different characteristics of planetary disks giving rise to terrestrial and giant planets. However, except for HD 217107, the five remaining stars in our sample with flat or negative slopes are currently known to have only one giant planet not on close-in orbits, with semimajor axes ranging from 0.50 to 2.20 AU (see Table 11), so these systems are compatible

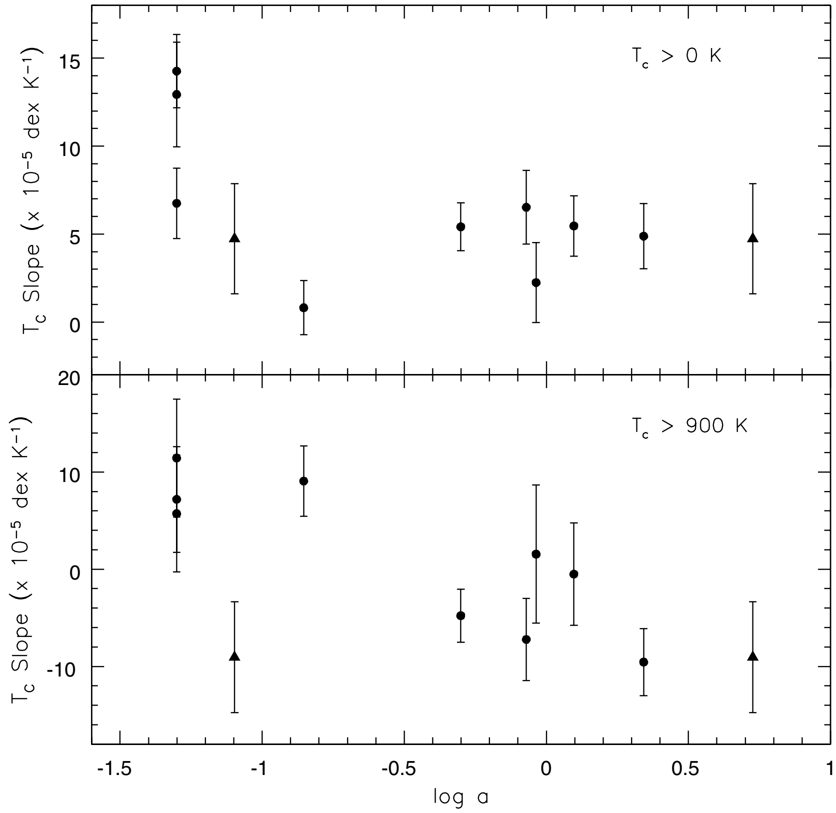

Figure 4. T_c slope as a function of the log of the semimajor axis (a) of the companion planet. The top panel shows the slopes in the [m/H]–T_c relations for all elements, and those for the refractory elements only ($T_c > 900$ K) are given in the bottom panel. The triangles represent the two planets orbiting HD 217107. The error bars represent the 1σ uncertainties in the slopes given in Table 10.

with the alternative explanation of M09. Also, Gonzalez et al. (2010) found that stars with giant planets have more negative slopes than stars without planets based on a sample of 65 of the former and 56 of the latter. Taken together, these results suggest that the fractionation of volatile and refractory elements may be a property of all planetary systems, with the refractory elements being locked up in either terrestrial or gas giant planets.

The lone star in our sample that is known to host at least two giant planets, HD 217107, is also consistent with this scenario. One planet, HD 217107 c, is on an extended orbit at 5.33 AU, while the second planet, HD 217107 b, is on a short orbit at 0.08 AU (Table 11). Despite having a close-in giant planet, the negative slope of HD 217107 implies that significant accretion of refractory-rich planet material did not take place in this system as HD 217107 b migrated to its current location. This further suggests that terrestrial planets did not form interior to HD 217107 b, and thus the fractionation of volatile and refractory elements occurs in the formation of terrestrial and gas giant planets alike. However, it is also possible that one or more terrestrial planets did form interior to HD 217107 b but were captured by the larger planet or scattered from their original orbits without accreting onto the host star during the planet's migration. This scenario would also conserve the deficiency of refractory elements in the star's photosphere, if in fact flat or negative T_c slopes result only from the formation of terrestrial planets.

While the flat or negative T_c slopes found for six stars in our sample are consistent with the planet signature scenario, the abundance trends may be the result of general chemical evolution of the Galaxy. In Figure 5(a), we plot the $T_c > 900$ K slopes as a function of [Fe/H] for the stars in our sample. Included in the figure is the standard linear least-squares fit to the similar slope versus [Fe/H] data for stars with and without known giant planets from Gonzalez et al. (2010, Table 1). The relation is similar to those in R09 and Ramírez et al. (2010); all of these studies find that the slopes become more negative at higher metallicities. If the relation is indicative of Galactic chemical evolution effects, negative slopes in metal-rich stars may not be a signature of planet formation. As seen in Figure 5(a), the six stars with flat or negative slopes studied here fall nicely along the fit to the Gonzalez et al. data, despite possible systematic differences in the T_c slopes between the two studies, and when the slopes are corrected for chemical evolution, the effect is clearer (Figure 5(b)). Tellingly, three of the four stars with close-in planets (HD 75289, HD 76700, and HD 195019) have slopes that lie above the Galactic trend by more than 2σ, providing additional evidence that these stars have accreted refractory-rich planetary material. The slope for HD 209458, the fourth star with a close-in planet, also lies above the trend but at a low confidence level ($\sim 1\sigma$).

5. SUMMARY

Stellar parameters and abundances of 18 elements have been homogeneously derived for 10 stars known to host Jovian-type giant planets. The LTE analysis is based on high-quality echelle spectroscopy obtained with the 9.2 m Hobby-Eberly and 2.2 m MPG/ESO telescopes. Stellar parameters were determined spectroscopically using the standard iterative technique. Abundances were derived from measured equivalent widths or synthesis of spectral lines and have internal uncertainties that

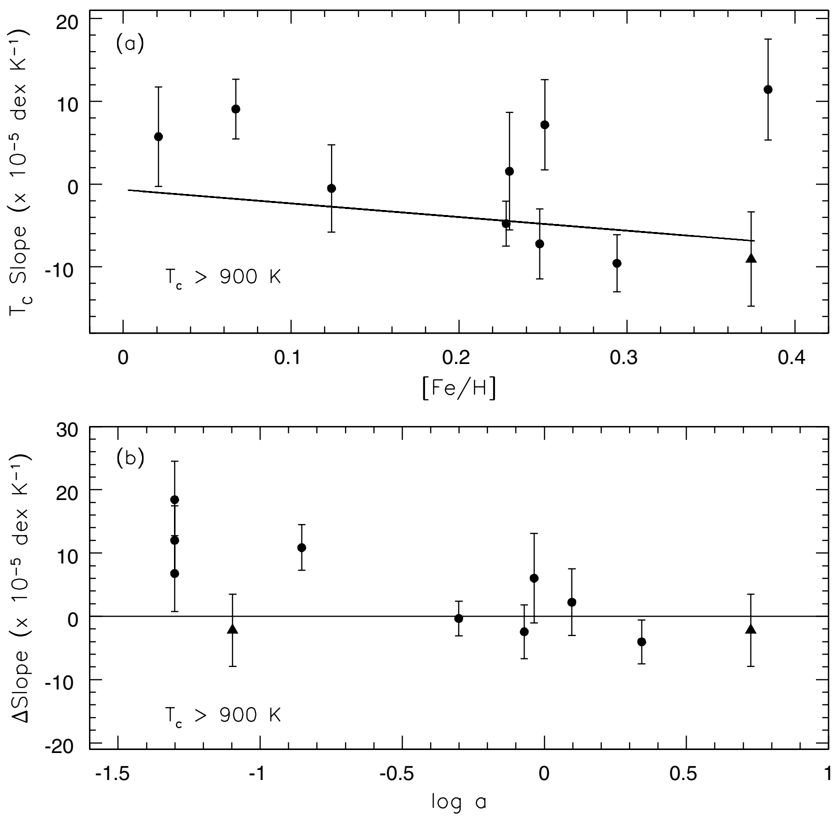

Figure 5. (a) T_c slope for the refractory elements ($T_c > 900$ K) as a function of [Fe/H]. HD 217107, the only star in our sample with two known planets, is given as the triangle. The solid line is the linear least-squares fit to the slope-[Fe/H] data for stars with and without known planets from Gonzalez et al. (2010) and defines the Galactic chemical evolution trend. (b) T_c slope for the refractory elements corrected for Galactic chemical evolution versus the log of the semimajor axis of the companion planet. The corrected slopes are the difference between the measured slope and the [Fe/H]-dependent fitted value for each star from the Galactic chemical evolution trend shown in panel (a). The two known planets of HD 217107 are again given as triangles.

are typically $\leqslant 0.05$ dex. Special attention was given to the derivation of the important volatile elements C, N, and O as well as the odd-*Z* elements Sc, V, Mn, and Co. Carbon abundances were derived from high-excitation C I and molecular C_2 lines, and the results from both features are in excellent agreement, with uncertainties in the mean abundances $\leqslant 0.03$ dex. Adopting the derived C abundances, N abundances were determined by analysis of three CN features in the λ6707 Li I region. Definitive measurements were possible for only four stars; upper limits are reported for the remaining six. Oxygen abundances have been derived from the λ6300 [O I] forbidden line and the high-excitation O I triplet with NLTE corrections from Takeda (2003). Differences in the abundances from the two features are $\leqslant 0.05$ dex. Account for hyperfine structure was taken in the derivation of Sc, V, Mn, and Co abundances. In most cases, the effect is less than 0.04 dex on the derived abundances; however, for the two most metal-rich stars in the sample, the difference is as high as 0.36 dex.

We have examined the abundances derived from our fine analysis as a function of condensation temperature of the elements to look for trends that may be related to the planet formation process. The precision of our abundances ($\leqslant 0.05$ dex) is of the order necessary to detect the potentially small abundance differences that may distinguish stars with and without planets. When considering the volatile and refractory elements together, we find positive slopes in the [m/H]–T_c relations for all 10 stars, in agreement with Smith et al. (2001) and Ecuvillon et al. (2006a). The slopes derived here are in general smaller (less positive) than those of S01 and E06 due primarily to systematic differences in the derived abundances. For seven stars, the [m/H]–T_c slopes fall along the trend of slope versus metallicity that defines the general chemical evolution of the Galaxy and thus do not appear to be indicative of planet formation around these stars. The remaining three stars—HD 75289, HD 76700, and HD 209458—have slopes lying above the Galactic evolution trend and are candidates for having accreted fractionated rocky material during the formation and/or evolution of their planetary systems.

It has been argued that volatile elements are more sensitive to Galactic chemical evolution effects than refractory elements and that trends with T_c of the latter are more robust when looking for a planet signature among stellar abundances (Ramírez et al. 2010). The slopes of the [m/H]–T_c relations for the refractory elements of our sample are dichotomized into groups with positive (four stars), and flat or negative (six stars) values. Positive slopes are a possible indication that there was no fractionation of volatile and refractory elements in the protoplanetary disks of the stars and thus terrestrial planet formation was suppressed. Alternatively, terrestrial planets or planet cores could have formed but were subsequently accreted onto the star due to dynamical processes in the disk, causing an enhancement in the photospheric abundances of the refractory elements. The four stars in our sample with positive T_c slopes have very close-in ($\leqslant 0.14$ AU) giant planets, which are thought to have migrated to their current locations after forming at larger radii. Three of these stars also have volatile + refractory T_c slopes lying above the general Galactic evolution trend, and all four lay above the Galactic trend for $T_c > 900$ K. These data strengthen the evidence that these four stars have undergone accretion of refractory-rich planet material.

Flat or negative T_c slopes for the refractory elements have been interpreted as a possible signature of terrestrial planet formation (Meléndez et al. 2009; Ramírez et al. 2009). Six stars in our sample with flat or negative T_c slopes—HD 2039, HD 20367, HD 40979, HD 52265, HD 89744, and HD 217107—are candidates for hosting terrestrial planets. However, the planet signature may not be limited to the formation of terrestrial planets but may result from the formation of gas giants, as well; this is evident by our sample of giant planet hosts. Furthermore, HD 217107, is the only star in our sample with two known planets; it has a 2.6 M_J planet orbiting at 5.33 AU and a 1.4 M_J planet orbiting at 0.08 AU. The negative T_c slope for this star suggests that fractionation of the refractory elements did occur and that significant accretion of refractory-rich planet material has not taken place despite having a Jovian-type giant planet on a close-in orbit. It seems then that the fractionation of volatile and refractory elements may be a process inherent to the formation of terrestrial and gas giant planets alike. However, interpretation of abundance trends may be complicated by Galactic chemical evolution effects. Larger samples of stars with and without known planets subject to a homogeneous abundance analysis based on high-quality spectroscopy are needed to determine definitively if the chemical abundance distributions of stars with known planets differ from the general stellar population.

S.C.S. acknowledges support provided by the NOAO Leo Goldberg Fellowship; NOAO is operated by the Association of Universities for Research Astronomy, Inc. (AURA), under a cooperative agreement with the National Science Foundation (NSF). D.F. was supported by the NOAO/KPNO Research Experiences for Undergraduates Program which is funded by the NSF Research Experiences for Undergraduates (REU) Program and the Department of Defense ASSURE program through Scientific Program Order No. 13 (AST-0754223) of the Cooperative Agreement No. AST-0132798 between AURA and the NSF. J.R.K. gratefully acknowledges support for this work by grants AST 00-86576 and AST 02-39518 from the National Science Foundation and by a generous grant from the Charles Curry Foundation to Clemson University. L.G. acknowledges the financial support from CNPq. The Hobby-Eberly Telescope (HET) is a joint project of the University of Texas at Austin, the Pennsylvania State University, Standford University, Ludwig-Maximilians-Universität München, and Georg-August-Universität Göttingen. The HET is named in honor of its principal benefactors, William P. Hobby and Robert E. Eberly. We thank the anonymous referee for helpful comments that have led to an improved paper.

Facilities: HET(HRS), Max Planck:2.2m(FEROS)

REFERENCES

Allende Prieto, C., Lambert, D. L., & Asplund, M. 2001, ApJ, 556, L63
Anders, E., & Grevesse, N. 1989, Geochim. Cosmochim. Acta, 53, 197
Asplund, M. 2005, ARA&A, 43, 481
Asplund, M., Grevesse, N., & Sauval, A. J. 2005a, in ASP Conf. Ser. 336, Cosmic Abundances as Records of Stellar Evolution and Nucleosynthesis, ed. T. Barnes & F. Bash (San Francisco, CA: ASP), 25
Asplund, M., Grevesse, N., Sauval, A. J., Allende Prieto, C., & Blomme, R. 2005b, A&A, 431, 693
Beirão, P., Santos, N. C., Israelian, G., & Mayor, M. 2005, A&A, 438, 251
Bensby, T., Feltzing, S., & Lundström, I. 2004, A&A, 415, 155
Bond, J. C., Tinney, C. G., Butler, R. P., Jones, H. R. A., Marcy, G. W., Penny, A. J., & Carter, B. D. 2006, MNRAS, 370, 163
Bubar, E. J., & King, J. R. 2010, AJ, 140, 293
Charbonneau, D., Brown, T. M., Latham, D. W., & Mayor, M. 2000, ApJ, 529, L45
Croll, B., et al. 2007, ApJ, 658, 1328
Ecuvillon, A., Israelian, G., Santos, N. C., Mayor, M., García López, R. J., & Randich, S. 2004a, A&A, 418, 703
Ecuvillon, A., Israelian, G., Santos, N. C., Mayor, M., & Gilli, G. 2006a, A&A, 449, 809 (E06)
Ecuvillon, A., Israelian, G., Santos, N. C., Mayor, M., Villar, V., & Bihain, G. 2004b, A&A, 426, 619
Ecuvillon, A., Israelian, G., Santos, N. C., Shchukina, N. G., Mayor, M., & Rebolo, R. 2006b, A&A, 445, 633
Fischer, D. A., & Valenti, J. 2005, ApJ, 622, 1102
Fitzpatrick, M. J., & Sneden, C. 1987, BAAS, 19, 1129
Ghezzi, L., Cunha, K., Schuler, S. C., & Smith, V. V. 2010a, ApJ, 725, 721
Ghezzi, L., Cunha, K., Smith, V. V., de Araújo, F. X., Schuler, S. C., & de la Reza, R. 2010b, ApJ, 720, 1290
Ghezzi, L., Cunha, K., Smith, V. V., & de la Reza, R. 2010c, ApJ, 724, 154
Gilli, G., Israelian, G., Ecuvillon, A., Santos, N. C., & Mayor, M. 2006, A&A, 449, 723
Gonzalez, G. 1997, MNRAS, 285, 403
Gonzalez, G. 1998, A&A, 334, 221
Gonzalez, G. 2006, MNRAS, 367, L37
Gonzalez, G., Carlson, M. K., & Tobin, R. W. 2010, MNRAS, 407, 314
Gonzalez, G., & Laws, C. 2000, AJ, 119, 390
Gonzalez, G., Laws, C., Tyagi, S., & Reddy, B. E. 2001, AJ, 121, 432
González Hernández, J. I., Israelian, G., Santos, N. C., Sousa, S., Delgado-Mena, E., Neves, V., & Udry, S. 2010, ApJ, 720, 1592
Henry, G. W., Marcy, G. W., Butler, R. P., & Vogt, S. S. 2000, ApJ, 529, L41
Huang, C., Zhao, G., Zhang, H.-W., & Chen, Y.-Q. 2005, Chin. J. Astron. Astrophys., 5, 619
Ida, S., & Lin, D. N. C. 2004, ApJ, 616, 567
Ida, S., & Lin, D. N. C. 2008, ApJ, 673, 487
Johansson, S., Litzén, U., Lundberg, H., & Zhang, Z. 2003, ApJ, 584, L107
Johnson, J. A., Ivans, I. I., & Stetson, P. B. 2006, ApJ, 640, 801
King, J. R., Deliyannis, C. P., Hiltgen, D. D., Stephens, A., Cunha, K., & Boesgaard, A. M. 1997, AJ, 113, 1871
Kiselman, D. 1991, A&A, 245, L9
Kupka, F., Piskunov, N., Ryabchikova, T. A., Stempels, H. C., & Weiss, W. W. 1999, A&AS, 138, 119
Kurucz, R. L., Furenlid, I., Brault, J., & Testerman, L. 1984, Solar Flux Atlas from 296 to 1300 nm, National Solar Observatory Atlas No. 1 (Cambridge, MA: Harvard Univ. Press)
Lambert, D. L., & Ries, L. M. 1981, ApJ, 248, 228
Laughlin, G., Marcy, G. W., Vogt, S. S., Fischer, D. A., & Butler, R. P. 2005, ApJ, 629, L121
Li, S.-L., Lin, D. N. C., & Liu, X.-W. 2008, ApJ, 685, 1210
Lin, D. N. C., Bodenheimer, P., & Richardson, D. C. 1996, Nature, 380, 606
Lodders, K. 2003, ApJ, 591, 1220
Luck, R. E., & Heiter, U. 2006, AJ, 131, 3069
Mandell, A. M., Ge, J., & Murray, N. 2004, AJ, 127, 1147
Mashonkina, L., Christlieb, N., Barklem, P. S., Hill, V., Beers, T. C., & Velichko, A. 2010, A&A, 516, A46
Mashonkina, L., Korn, A. J., & Przybilla, N. 2007, A&A, 461, 261
Mayor, M., & Queloz, D. 1995, Nature, 378, 355
Mazeh, T., et al. 2000, ApJ, 532, L55
McDonough, W. F. 2001, in The Composition of the Earth, in Earthquake Thermodynamics and Phase Transitions in the Earth's Interior (International Geophysics Series, Vol. 76), ed. R. Teisseyre & E. Majewski (San Diego, CA: Academic Press), 5
Meléndez, J., Asplund, M., Gustafsson, B., & Yong, D. 2009, ApJ, 704, L66 (M09)
Miller-Ricci, E., et al. 2008, ApJ, 682, 586
Moldovan, R., Matthews, J. M., Gladman, B., Bottke, W. F., & Vokrouhlický, D. 2010, ApJ, 716, 315
Murray, N., & Chaboyer, B. 2002, ApJ, 566, 442
Nissen, P. E., & Edvardsson, B. 1992, A&A, 261, 255
Pinsonneault, M. H., DePoy, D. L., & Coffee, M. 2001, ApJ, 556, L59
Piskunov, N. E., Kupka, F., Ryabchikova, T. A., Weiss, W. W., & Jeffery, C. S. 1995, A&AS, 112, 525
Prochaska, J. X., & McWilliam, A. 2000, ApJ, 537, L57
Ramírez, I., Allende Prieto, C., & Lambert, D. L. 2007, A&A, 465, 271
Ramírez, I., Asplund, M., Baumann, P., Meléndez, J., & Bensby, T. 2010, A&A, 521, A33
Ramírez, I., Meléndez, J., & Asplund, M. 2009, A&A, 508, L17 (R09)
Rich, J. A., & Boesgaard, A. M. 2009, ApJ, 701, 1519
Ryabchikova, T. A., Piskunov, N. E., Stempels, H. C., Kupka, F., & Weiss, W. W. 1999, Phys. Scr., T83, 162

Sadakane, K., Honda, S., Kawanomoto, S., Takeda, Y., & Takada-Hidai, M. 1999, PASJ, 51, 505
Santos, N. C., Israelian, G., & Mayor, M. 2001, A&A, 373, 1019
Santos, N. C., Israelian, G., & Mayor, M. 2004, A&A, 415, 1153
Schuler, S. C., Hatzes, A. P., King, J. R., Kürster, M., & The, L.-S. 2006, AJ, 131, 1057
Schuler, S. C., Plunkett, A. L., King, J. R., & Pinsonneault, M. H. 2010, PASP, 122, 766
Smith, V. V., Cunha, K., & Lazzaro, D. 2001, AJ, 121, 3207 (S01)
Sneden, C. 1973, ApJ, 184, 839
Sneden, C., Kraft, R. P., Prosser, C. F., & Langer, G. E. 1991, AJ, 102, 2001
Takeda, Y. 2003, A&A, 402, 343
Takeda, Y., & Honda, S. 2005, PASJ, 57, 65
Takeda, Y., et al. 2001, PASJ, 53, 1211
Thevenin, F. 1990, A&AS, 82, 179
Vauclair, S. 2004, ApJ, 605, 874